# Refining the delivery and therapeutic efficacy of cetuximab using focused ultrasound in a mouse model of glioblastoma: An 89Zr-cetuximab immunoPET study

Estelle Porret, Dimitri Kereselidze, Ambre Dauba, Arnaud Schweitzer-Chaput, Benoit Jegot, Erwan Selingue, Nicolas Tournier, Benoît Larrat, Anthony Novell, Charles Truillet

# Refining the delivery and therapeutic efficacy of cetuximab using focused ultrasound in a mouse model of glioblastoma: an $^{89}$Zr-cetuximab immunoPET study.

Estelle Porret,[1] Dimitri Kereselidze,[1] Ambre Dauba,[1] Arnaud Schweitzer-Chaput,[1] Benoit Jegot,[1] Erwan Selingue,[2] Nicolas Tournier,[1] Benoît Larrat,[2] Anthony Novell,[1] Charles Truillet[1,*]

1 Université Paris-Saclay, CEA, CNRS, Inserm, BioMaps, Service Hospitalier Frédéric Joliot, 4 place du général Leclerc, 91401, Orsay, France
2 Université Paris-Saclay, CEA, CNRS, NeuroSpin/BAOBAB, Centre d'études de Saclay, Bâtiment 145, 91191 Gif sur Yvette, France

* : corresponding Author, charles.truillet@universite-paris-saclay.fr, + 33 (0)1 69 86 77 27

# ABSTRACT

**Introduction:** Glioblastoma (GBM) is the most common and deadly form of primary brain tumor. Between 30% and 60% of GBM are characterized by overexpression of the Epidermal Growth Factor Receptor (EGFR). The anti-EGFR antibody Cetuximab (CTX) showed favorable effect for EGFR$^+$ colorectal cancer but failed to demonstrate efficacy for GBM. Insufficient CTX passage through the blood-brain barrier (BBB) and limited and non-homogenous delivery of CTX into the tumor, probably linked to heterogeneity in the permeability of the blood-tumor barrier (BTB), is assumed to be the main determinant of the limited efficacy of this immunotherapy.
**Objective:** Using PET imaging, we have previously demonstrated that focused ultrasound (FUS) combined with microbubbles (µB) allowed significant and persistent delivery of CTX across the BBB in healthy mice. We here investigated the delivery of radiolabeled CTX and the impact for therapeutic efficacy of CTX immunotherapy combined with FUS in an orthotopic GBM mice model.
**Methods:** After radiolabeling CTX with the long half-life isotope $^{89}$Zr, PET images have been acquired overtime in mice bearing U251 (EGFR$^+$) with or without FUS treatment. Autoradiography combined with immunofluorescence staining were used to understand FUS impact on CTX distribution. A survival study was conducted simultaneously to evaluate the therapeutic benefit of repeated CTX monotherapy associated or not with FUS.
**Results:** *Ex vivo* analysis confirmed that FUS allowed for a clear enhancement of the delivery of CTX into all the FUS exposure area, including the tumor and the contralateral hemisphere, until 24h post-injection. Interestingly, FUS did not improve the accumulation and retention of CTX into the tumor compared with the control group (no FUS). No significant difference in the CTX treatment efficacy, determined by the survival between FUS and non-FUS group, was observed. This result is consistent with the absence of FUS-induced change in the delivery of CTX in the tumor. Moreover, no significant change in neuroinflammation potentially induced by the FUS was observed in the area surrounding the tumor.
**Conclusion:** Taking together, these data suggest that FUS combined with µB may homogenize the delivery of CTX into the tumor and might activate glial cells. In this specific model, enhanced delivery of CTX did not improve the survival of GBM mice compared with CTX treatment alone, even after multiple therapeutic sessions.

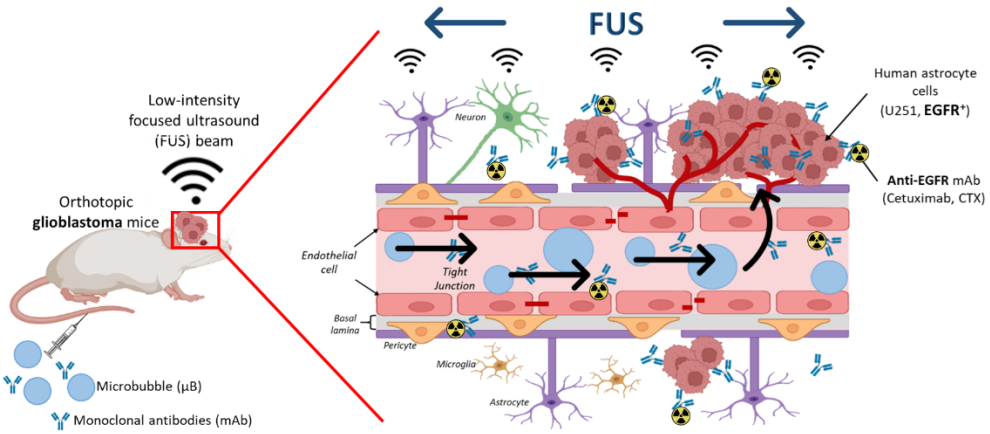


# INTRODUCTION

Glioblastoma multiforme (GBM) is the most common and deadly form of primary brain tumor with an incidence ranging from 0.59 to 5 per 100,000 persons worldwide.[1] Overexpression of the Epidermal Growth Factor Receptor (EGFR-wt) and its mutant, especially EGFR-variant III (EGFR-vIII), occurs in ~ 50% of GBM.[2] EGFR was shown to promote the development of the tumor by increasing cellular proliferation, angiogenesis, metastasis and reducing apoptosis. In this context, anti-EGFR monoclonal antibodies (mAb) such as cetuximab (IMC-C225, CTX), which specifically bind to the extracellular domain of the receptor to block the EGFR signaling pathways, have emerged as promising therapeutics in GBM.[2][3]

CTX, a human-murine chimeric monoclonal anti-EGFR antibody, have raised some interest since it binds to EGFR-wt and EGFR-vIII with the same affinity.[5] Clinical trials with single CTX treatment or in combination with routine chemotherapy or radiotherapy in patient with squamous cell carcinoma of the head and neck[6] or metastatic colorectal cancer[6][7][8] reported improvements in overall survival and objective responses rate, without additional negative impact on the quality of life. In a preclinical study on nude mice subcutaneous implanted with GBM cells, repeated CTX treatments significantly improved the overall survival and reduced the tumor volume, or even induced complete therapeutic response with disappearance of the tumor.[9] However the clinical trials in GBM failed to demonstrate any efficacy despite high $EGFR^+$ expression.[10] The presence of intact blood-brain barrier (BBB), which drastically restricts the passage of mAb into the brain appears as the main hypothesis for limited treatment efficacy.[11] The growth of GBM is accompanied by the development of abnormal tumor vasculature forming the blood-tumor barrier (BTB)[11] which can be somewhat leaky and may allow the extravasation of mAb.[12] However, the magnitude of BTB alteration within the tumoral lesion is highly heterogeneous and depends on the development stages of the tumor and the tumor core or its periphery structure.[13][14] Several studies have shown that the delivery of mAb in GBM is sub-optimal in term of therapeutic concentration, exposure time, and tumor whole diffusion.[10][12][15] For all these reasons, CTX treatment alone has never reached more than phase II clinical trials for the treatment of GBM.[10][15]

Few strategies have been proposed in preclinical models and clinical trials to overcome the BTB and improve therapeutic efficacy in GBM such as the implantation of intracranial catheter to deliver CTX directly into the tumor of orthotopic xenograft mice[15] and the intra-arterial cerebral infusion of mannitol followed by CTX[16][17]. In this framework, the combination of intravenous injection of microbubbles (µB) with low-intensity focused ultrasound (FUS) appeared as a promising non-invasive technique to transiently disrupt the BBB/BTB.[19][20] The mechanical interaction between the ultrasound, the µB, and the vasculature was shown to disassemble the tight junction and enable the transport of molecules across the BBB, thus improving drug delivery to the brain. This procedure offers several advantages: its repeatability, its compatibility with currently approved drugs and its selectivity by targeting only specific brain regions.

Recent studies have shown that FUS-induced BBB opening resulted in improved delivery of mAb, such as trastuzumab (TRZ, anti-HER2)[20], CTX[21] and bevacizumab (BVZ, anti-VEGFR)[22], in healthy mice brains. The therapeutic benefits of this method currently under investigation in preclinical models seem to be more heterogeneous. In orthotopic human GBM cell lines (U87-MG) mouse model, Hao-Li Liu *et al.* demonstrated a 2.8 fold increase of the median survival time for the mice treated with FUS combined with BVZ compared to the once treated with BVZ only.[22] In the opposite, the combination of FUS with TRZ did not result in a survival increase of brain metastasis bearing rats.[23][24] The survival curves between the TRZ alone and the FUS combined with TRZ treatment groups were significantly different from the control group but did not differ among themselves. It may be hypothesized that response to the treatments may be linked with the quality of BBB/BTB disruption, which comes from a different micro-vasculature.

Some groups have exploited an additional effect of FUS based on local induction of a neuroimmune response as a therapeutic axis. It has been reported that FUS is able to activate microglia and then astrocytic cells in healthy rodents.[25][26] FUS is therefore likely to transiently activate the glial cells surrounding the tumor which may help fighting tumor cells. However, a holistic view of this neuroglial activation additional impact of FUS with the enhancement of drug delivery is currently missing.

ImmunoPET method, combining sensitivity with positron emission tomography (PET), and the specificity of mAbs as the biomarker of interest appears as a promising and translational approach for quantitative and longitudinal follow-up of the diffusion of therapeutic mAb in healthy and cancerous tissues.[27] In a previous study, our group demonstrated that FUS-induced BBB opening allowed significant and persistent delivery of radiolabeled CTX in the brain of healthy mice.[28] In the present study, we investigated the synergistic efficacy of repeated CTX therapies combined with FUS on a nude GBM mouse model. This study is focused on the therapeutic potential of the transient disruption of the BBB/BTB induced by FUS and μB to (i) exacerbate the CTX effect by increasing its concentration and/or homogenized its delivery, and (ii) to activate surrounding glial cells. Glial cells activation was assessed by TSPO-PET imaging, a biomarker of the neuroinflammation, thanks to a specific TSPO radioligands the $^{18}$F-DPA-714.

# 1. METHODS

## 1.1 Materials

Gentisic acid ($C_7H_6O_4$ and purity ≥ 98%), sodium acetate trihydrate ($CH_3COONa,3H_2O$ ≥ 99%), citric acid monohydrate ($C_6H_6O_7,H_2O$ ≥ 99%), ammonium chloride ($NH_4Cl$ ≥ 99.5%), phosphate buffered saline (PBS) tablette, tris buffered saline, evans bleu, bovin serum albumin, tween 20, triton, paraformaldehyde, bicinchoninic acid protein assay kit, acetone, dimethyl sulfoxide anhydrous were purchased from Sigma-Aldrich (France). Sodium carbonate ($Na_2CO_3$) and bone wax were purchased from VWR (France). Erbitux (Cetuximab, CTX, 5 mg/mL) and p-isothiocyanatobenzyldesferrioxamine were purchased from Merck (Belgium) and Macrocyclics (USA). 89-Zirconium [$^{89}$Zr]Zr-oxalic acid was obtained from PerkinElmer (the Netherlands). $H_2O$ Optimal LC/MS and 2-Methylbutan were purchased from Fisher chemical (Thermo Fisher Scientific, France) and Honeywell (France). Methanol and acetonitrile were obtained from Carlo Erba (France). Saline solution (0.9%) and isoflurane were purchased from Baxter (France). PD-10 desalting columns and instant thin-layer chromatography on glass microfiber chromatography paper impregnated with silica gel were purchased from GE Healthcare (France). Vivaspin® ultrafiltration tubes (5 kDa) were obtained from Sartorius (France). Prolong Diamond Antifade Mountain with DAPI was purchased from Invitrogen (Thermo Fisher Scientific, France) and optimum cutting temperature from Cell Path (United Kingdoms). Dulbecco's phosphate buffered saline (10 mM), HEPES buffer, Trypsin-EDTA, antibiotic-antimycotic, fetal bovine serum and cell culture medium (Dulbecco's Modified Eagle's medium) were purchased from Gibco (Thermo Fisher Scientific, France). Mini-PROTEAN TGX gels 4-15%, Trans-blot turbo midi format 0.2µm PVDF, Tris-glycine buffer, Clarity Western ECL Substrate were purchased from Bio-Rad (France). Halt protease and phosphatase inhibitor cocktail was purchased from Thermo Scientific (Thermo Fisher Scientific, France). Ketamine (Imalgene), Xylazyne (Rompun) and Xylocaïne were purchased from Mérial, Bayer and Aspen respectively. Suturing thread was purchased from Filapeau (France). Microbubbles (SonoVue®, $1.5 \times 10^8$ µB/mL) were purchased from Bracco (Milan, Italy) Distilled water was purified using a Milli-Q system greater than 18 MΩ cm resistance (Millipore, France) for all immunohistological buffers. All products were used as received without further purification.

## 1.2 Preparation of 89-Zirconium Cetuximab ($^{89}$Zr-CTX)

### 1.2.1 Buffer exchange

The storage buffer of CTX, that could perturbated the functionalization with desferrioxamine (DFO), was removed by centrifugated third times (5,500 rpm, 4°C, 90 minutes (min) on a 5804R centrifuge from Eppendorf) CTX with normal (0.9%) saline solution through Vivaspin® ultrafiltration tubes (5 kDa cutoff). The final concentration of CTX solution (25 mg/mL) was determined by measuring the absorption at 280 nm on a spectrophotometer (CLARIO Start Plus, BM6 LABTECH).

### 1.2.2 Functionalization of CTX with p-NCS-Bz-DFO and radiolabeling with $^{89}$Zr

CTX was radiolabeled with $^{89}$Zr using p-isothiocyanatobenzyldesferrioxamine (p-NCS-Bz-DFO) as chelate following the protocol in the Vosjan *et al.*[29] Briefly, 17 µL of p-NCS-Bz-DFO (10 mM in DMSO) was mixed in steps of 2-3 µL using a thermomixer at 550 rpm into CTX solution (5 mg in 1 mL), adjusted at pH 9.3 with sodium carbonate ($Na_2CO_3$, 0.1 M). The molar ratio CTX to DFO was 1:5. The solution was stirred during 45 min at 37°C to complete the reaction. The purification was done through a PD-10 column using sodium acetate trihydrate buffer (0.25 M, pH 5.4-5.6) containing gentisic acid (5 mg/mL) as mobile phase. The purified CTX functionalized with DFO (CTX-DFO) solution was stored at -20°C until radiolabeling.

On the day of imaging experiments, 1.5 mg of CTX-DFO solution (600 µL) was used for the radiolabeling process and the pH was adjusted to 7.2 by adding 1 mL of HEPES solution (0.5 M). The oxalic acid of the $^{89}$Zr solution (220 µL, 6 mCi) was neutralized with 100 µL of $Na_2CO_3$ (2 M) before adding them to the CTX-DFO solution. The solution was stirred for 1 hour (h) at 37°C and 300 rpm to

complete the reaction. $^{89}$Zr-CTX was purified through PD-10 column using HEPES solution (0.5 M) and concentrated by Vivaspin® ultrafiltration tubes (5 kDa cutoff).

#### 1.2.3 $^{89}$Zr-CTX characterization

The radiochemical yield and purity were determined using instant thin-layer chromatography on glass microfiber chromatography paper impregnated with silica gel (iTLC-SG) as stationary phase and citric acid solution (20 mM, adjusted at pH 4.9–5.1 with $Na_2CO_3$ (2 M) with 10% of acetonitrile as mobile phase. The migration was followed by radio-TLC detection (Mini-Scan TLC Imaging Scanner, Eckert&Ziegler,Berlin, Germany).

Size exclusion high performance liquid chromatography (SE-HPLC) measurements of $^{89}$Zr-DFO-CTX and CTX were performed on a Dionex system (ThermoFisher Scientific, France) with a P680HPLC pump, a thermostatted column compartment (TCC-100 at 30°C), a UV-vis (UVD170U UV/VIS) and a scintillation detector (Packard, Canberra, Austria). SE-HPLC was performed using a bioZen 1.8 µm SEC-2 LC column (Phenomenex, France). A linear-gradient elution was carried out with a solution of KH2PO4 (50 mM) and KCl (250 mM) (pH 6.8), at a flow rate of 0.2 mL/min. Eluted species were detected via a UV detection and radioactivity detection.

## 1.3 Cell culture

The human U251 cells derived from human astrocyte GBM grade III-IV were chosen as EGFR-positive model, because the specific interaction with CTX was already validated *in vitro*[30][31] and *in vivo*[31]. They were purchased from Sigma-Aldrich (No. 89081403). Cells were cultured in a humidified incubator (Sanyo, Japan) at 37°C in an atmosphere containing 5% of $CO_2$ in DMEM (Dulbecco's Modified Eagle's medium) supplemented with 10% of heat-inactivated FBS (Fetal Bovine Serum), 1% antibiotic-antimycotic (Streptomycine, amphotéricine B, pénicilline). Mycoplasma absence was confirmed using MycoAlert™ kit (Lonza, USA).

## 1.4 Western Blot experiment

Translocator protein (TSPO) and EGFR expression in the U251 human GBM cell line was evaluated by western blot analysis. U251 cells were lysed using cell signaling kit completed with protease and phosphatase inhibitor cocktail. Total protein concentration in cell lysates was determined by a bicinchoninic acid protein assay. Equal amounts (20 µg) of total proteins were separated using 4-15% Mini-PROTEAN TGX gels with SDS-PAGE and then transferred to a polyvinylidene fluoride (PVDF) membrane by semi-dry blotting. After transfer, blots were immersed in blocking solution (5% of Bovin Serrum Albumin, BSA and 0.1% of Tween-20 in Tris Buffered Saline (TBS) for 2h at Room Temperature (RT). The blots were then incubated overnight at 4°C with the following primary antibodies diluted at 1:100 in blocking solution: rabbit anti-human/mouse TSPO (Abcam, clone EPR5384, ab109497) and rabbit anti-human/mouse EGFR (ThermoFisher, clone PA5, PA5-85089). After washing three times with 0.1% Tween-20 in TBS, blots were incubated 1h at RT with an HRP-conjugated donkey anti-rabbit secondary antibody diluted at 1:10,000 in blocking solution (Jackson ImmunoResearch 711-035-152). Proteins were detected using the clarity western ECL substrate. After washing, immunoblots were imaged with the FUSION FX imaging system (Vilber, France). Image post-processing (cropping, global contrast adjustment) was performed with ImageJ software (v1.53i).

## 1.5 Animal experiments

Animal experiments were conducted in accordance with the European Directive 2010/63/EU on the protection of laboratory animals (French la transposition: Decree No. 2013-118). The protocols were approved by the Ethical Committee (authorization D91–471-105, ethics committee: CETEA-CEA DSV IdF).

In total, 59-female athymic NMRI (Naval Medical Research Institute) nude mice five-week-old were purchased from Janvier laboratories (Le Genet sur Isle, France, Mus musculus, NMRI-FOXN1 Nu/Nu), for therapeutic and imaging protocol as illustrated in figure S2&S4 and for the preliminary FUS

implementation (n=2). Mice were housed four per cage with food and water ad libitum in an environmental enrichment (polycarbonate cottages and wooden stocks), in a temperature (22°C) and humidity (40%) controlled room and were maintained under specific pathogen-free conditions.

## 1.6 Orthotopic glioblastoma tumor model

For intracranial tumor establishment, mice were anesthetized with isoflurane anesthesia in 100% of $O_2$ (4% for induction and 2% for maintenance) associated with xylocaïne in local. A small incision on the brain skin was made. A Hamilton syringe was used to slowly (0.6 µL/min) inject 1.5 x $10^6$ U251 cells suspended in 3 µL of dulbecco's phosphate buffered saline (D-PBS) into the striatum (at 2 mm lateral to the sagittal suture of the bregma and 3 mm below the dura). The syringe was left in place 5 min before to be slowly retracted (0.05 mm/min). The skull was sealed with bone wax and the incision was closed with suturing thread. Animal weight was monitored three times a week. The tumors were allowed to grow during 11-28 days before the different imaging sessions or the survival study begin.

## 1.7 FUS-induced BBB permeabilization

### 1.7.1 FUS procedure

Animal experiments were performed under Isoflurane anesthesia (4% for induction and 2% for maintenance) in a mixture of air and oxygen (air: 80% with pure $O_2$: 20%). The FUS procedure was similar to the protocol already validated on healthy mice and published by Tran *et al.*[28] Briefly, FUS were delivered using a focused transducer (active diameter 25 mm, focal depth 20 mm, Imasonic, Voray sur l'Ognon, France) centered at 1.5 MHz connected to a programmable generator (Image Guided Therapy, Pessac, France). The transducer was mounted on a motorized XYZ-axis stage and coupled to the mouse skull using a latex balloon filled with deionized and degassed water and coupling gel. A 100 µL bolus of SonoVue® were intravenously administered in the tail vein. A mechanical zig-zag shaped scan (XY-axis) was synchronized to the generator output in order to induce a wide BBB opening covering a cubic region in the middle of the brain of 6 mm x 6 mm x 7 mm (**Figure S1**). Ultrasonic waves were transmitted at 1.5 MHz during the transducer translation with a duty cycle of 69%. FUS protocols at high duty cycle combined with raster scan have been already validated in multiple mice studies.[33][34] The trajectory was repeated 25 times for a total exposure of 127 seconds (s). For the FUS group, the transmitted *in situ* peak negative pressure in the mouse brain was estimated to be 430 kPa at 1.5 MHz. The protocol was similar for the sham group for which the acoustic pressure was set 0 kPa.

### 1.7.2 Evan's blue extravasation test

The FUS-induced BBB opening was validated using the Evan's blue extravasation assay on a mouse. Microbubbles (100 µL of SonoVue®) were administrated intravenously. Right after FUS exposure (described in 1.7.1) ended, the BBB integrity marker (100 µL of Evans bleu at 4% in D-PBS) was injected intravenously. One hour later, the mouse was sacrificed by cervical dislocation under isoflurane (5%). Brain was removed, sectioned and pictures were taken.

## 1.8 PET acquisition and images reconstruction

PET acquisitions were performed using the Inveon microPET-CT (Siemens Medical Solutions, Knoxville, TN, USA). The spatial resolution of the PET scanner is ~ 1.5 mm (FWHM). After the PET scan, a 6min 80kV/500µA CT scan was performed for attenuation correction. PET images were reconstructed using a 3D OSEM iterative algorithm (4 iterations, 16 subsets, voxel size = 0.4 mm x 0.4 mm x 0.8 mm). Normalization, dead time correction, randoms subtraction, CT-based attenuation and scatter corrections were applied.

## 1.9 Study design

### 1.9.1 Longitudinal PET evaluation of $^{89}$Zr-CTX brain delivery with and without FUS-induced BBB/BTB in GBM

Imaging protocol and tissue section process:

28 days after tumor implantation, a total of 12 mice were randomized into 2 groups that received intravenous co-injection of SonoVue (100 µL) and $^{89}$Zr-CTX (100 µL, 40 mg/kg, 3.7 MBq) followed by: FUS exposure (n=6) or not (n=6). A 20min PET acquisition was performed immediately, 4h, 24h, 48h, 72h and 7 days after FUS exposure. One mouse per group was sacrificed by cervical dislocation under isoflurane (5%) 24h post-injection. Brains were removed, immersed in 2-methylbutan and frozen in liquid nitrogen. Serial coronal brain sections were cut throughout the striatum of the frozen brain at 14 µm with a cryostat (Leica CM3050 S, Leica biosystems) and adhered on SuperFrost Ultra Plus TM slides (FisherScientific). Slides were stored at -80°C until histological analysis (hematoxylin-eosin, auto-radiography and immunofluorescence staining). The timeline of the experiments is shown in **Figure S2A and B**.

Image analysis:

Imaging analyses were performed with the PMOD software (Version 3.9, Switzerland). All the images and extracted data were corrected according to the half-life of $^{89}$Zr ($t_{1/2}$=3.3 days). A volume of interest (VOI) of 6.4 mm$^3$ placed in the middle of the cerebellum was used as the region of reference. Indeed, cerebellum was not exposed to FUS and $^{89}$Zr-CTX retention remained constant over time (**Figure S3**). A threshold (mean of the concentration of activity in the cerebellum + twice the standard deviation) was applied into the PET images in order to suppress the background and facilitate the localization of the tumor volume. The $^{89}$Zr-CTX accumulation in the tumor was measured by positioning a VOI of 13.3 mm$^3$ on the middle of the tumor. Then, the VOI was mirrored to the contralateral side to estimate $^{89}$Zr-CTX accumulation in a non-sonicated volume. The activities were expressed using the following formula in SUV.

### 1.9.2 Longitudinal PET evaluation of brain inflammation using TSPO ligand ($^{18}$F-DPA-714) in healthy mice

Imaging protocol:

Healthy mice (n=6) underwent $^{18}$F-DPA-714 scans 7 days before FUS protocol, and at different time after FUS opening (15min, 48h, 72h (n=5) and 192h (n=5)). Repeated scans were performed on the same animals whenever possible. $^{18}$F-DPA-714 was synthesized as previously described.[34] Mice were anesthetized with isoflurane Dynamic PET scans of 60min (framing: 3x30s, 5x60s; 5x120s, 3x180s, 3x240s, 4x300s, 1x240s) were acquired after injection into the tail vein performed under the PET scanner. The injected dose was 280±50.3 MBq/kg of $^{18}$F-DPA-714 (injected mass: 0.086±0.03 nmol; volume: 100 µL).

Image analysis:

Each PET image was cropped around the skull and semi-automatically registered to an MRI atlas.[35] PET image analysis was performed using PMOD. PET quantification was performed on the different organs of interest, particularly the brain. VOI was delineated manually on the FUS site and on the cerebellum, used as a reference organ without FUS impact.

### 1.9.3 Therapeutic efficacity of CTX combined with FUS treatment.

The survival study performed in mice was designed in aim to mimic the multiple treatment sessions which corresponds to the schedule that patient would receive. The timeline of the experiments is shown in **Figure S4A and B**.

Eleven days after tumor implantation, a total of 37 mice were randomized into 4 groups that received either: (i) only µB (n=6), (ii) µB followed by FUS exposure (n=6), (iii) µB and CTX treatment (n=12), (iv) µB and CTX treatment followed by FUS exposure (n=13). The CTX (40 mg/kg, 40 µL) and µB (SonoVue, 100 µL) were intravenously injected twice per week for a total of 5 sessions.

Animal endpoint according to a scoring establish by our lab taking into consideration the behavior, the body-score and the general aspect of the animals was used to determine the survival. Mice were

euthanized by cervical dislocation. Kaplan-Meier survival curves were plotted with the use of GraphPad Prism software (GraphPad Software, San Diego, CA), and median survival was calculated.

#### 1.9.4 Brain inflammation assessed using $^{18}$F-DPA-714 PET imaging under CTX and FUS treatment

PET imaging was performed on few mice per treatment group, as represented on the timeline of the experiments (**Figure S4A and B**).

Imaging protocol:

Two days after the last treatment, $^{18}$F-DPA-714 was intravenously injected (250 ± 60 MBq/kg) followed by a 60min dynamic PET scan acquisition as already described. After 24h, one mouse from the group (iii) and one from the group (iv) were anesthetized with intraperitoneal injection of Ketamine (0.1 mg/g)/Xylazyne (0.1 mg/g) and were transcardially perfused with 20 mL of normal (0.9%) saline solution. Brains were removed, embedded in optimum cutting temperature tissue-mounting medium, frozen in liquid nitrogen and stored at -80°C until the day of sectioning. Coronal brain sections were cut at 16 µm for immunofluorescence staining.

Image analysis:

As previously described, imaging analyses were performed with the PMOD software. Extracted data were corrected according to the half-life of $^{18}$F ($t_{1/2}$=109.8min) and expressed as SUV. The mean of the concentration of activity (%ID/cc) in the cerebellum plus twice the standard deviation was used as threshold to facilitate the manual determination of the volume of $^{18}$F-DPA-714 accumulation in the tumor hemisphere. Then, the VOI was horizontally displaced in the contralateral side and eventually reduce to obtain the $^{18}$F-DPA-714 accumulation in the contralateral.

## 1.10 Histological analysis

#### 1.10.1 Autoradiography

Slides were exposed to a storage phosphor screen (VWR) in an exposure cassette (Molecular Dynamics) for 72h at RT. The screen was developed with Storm 860 Molecular Imager at 50 µm resolution. Images were analyzed using ImageJ software (v1.53i) and corrected according to the half-life of $^{89}$Zr.

#### 1.10.2 Hematoxylin-eosin staining

Slides with frozen brain sections were fixed in neutral buffer formalin 10% for 30min then washed with distilled water. Standard hematoxylin and eosin (H&E) staining was performed using Harris hematoxylin and Eosin Y alcoholic (Sigma-Aldrich). Transmitted light images of stained tumor sections were acquired with the Axio Observer 5 microscope (Zeiss, Germany) at 20X magnification. Image post-processing was performed with the ZEN software (v2.6, Zeiss).

#### 1.10.3 Immunofluorescence staining

Frozen brain sections were fixed in neutral buffer formalin 10% for 15min at RT, then washed 5min with PBS buffer. The neutral buffer formalin 10% effect were inactivated by incubating the sections in ammonium chloride solution (50 mM in PBS), then washed 5min with PBS buffer. Sections were successively immersed during 5min at RT in permeabilized solutions: MeOH/acetone (V/V = 1/1) and Triton solution (0.1% in PBS), then washed 5min with PBS buffer. Sections were immersed in blocking solution (5%BSA, 0.5% Tween-20 solution in PBS) for 1h at RT.

To determine astrocyte and microglial expression of TSPO *in vivo*, fluorescent colocalization was used.

Sections were incubated 1h at RT with relevant primary antibodies diluted at 1:100 in blocking solution: rabbit anti-PBR for TSPO (EPR5384, NOVUS, NBP1-9567), chicken anti-GFAP for astrocytes (Abcam, ab4674), goat anti-CD11B for microglia (antibodies online, ABIN284101)). After washing three times with PBS, sections were incubated 30min at RT with secondary antibodies diluted at 1:1000 in blocking solution: donkey anti-rabbit 546 (Life Tech, A10040), goat anti-chicken 647 (Invitrogen, A21449), goat anti-rat 488 (Invitrogen, A11006). The presence of human U251 cells was revealed on adjacent brain sections by additional incubation (90min at RT) with mitochondria mouse

anti human Alexa 488 (Sigma-Aldrich, clone 113, MAB1273A4) or EGFRp rabbit anti-human Alexa 647(Abcam, phospho Y106, EP774Y, Ab205828) diluted at 1:100 in blocking solution. Slides were washed with PBS buffer before to be mounted using Prolong Diamond Antifade Mountain with DAPI. Fluorescence microscopy was performed on Axio Observer 5 microscope (Zeiss, Germany) at 20X and 40X magnifications. Qualitative analyses were performed with ImageJ software (v1.53i). The nonspecific background stain was suppressed by applying a threshold (mean of the fluorescence intensity in the contralateral hemisphere plus two times the standard deviation).

## 1.11 Statistical analysis

All data are presented as mean ± standard deviation. The statistical analyses were performed using GraphPad Prism software (Graph Pad software Inc., San Diego, USA). Comparisons of PET data between FUS and Non FUS over time were performed using unpaired t-test. Mantel-Cox log-rank test was used for statistical significance of intergroup comparisons. Changes at the 95% confidence level ($p<0.05$) were qualified as statistically significant.

# 2. RESULTS

## 2.1 Validation of the radiolabeling of $^{89}$Zr-CTX and the FUS protocol on BBB permeation and safety.

CTX was successfully radiolabeled with $^{89}$Zr with high radiochemical yield (~ 60% for the crude product) before purification and the after purification, the radioligand purity was above 95% as confirmed on iTLC and HPLC measurements **(Figure SI5).**

The capacity of µB intravenously injected followed by FUS exposure to induce BBB/BTB was confirmed by the obvious presence of Evans blue in the sonicated brain, as illustrated in **Figure S6.** This FUS protocol was previously validated on healthy mice, no brain damage was observed using T2 MRI and gross pathology.[28]

## 2.2 FUS enables an increase of early extravasation of $^{89}$Zr-CTX but does not improve overall tumor accumulation in a GBM mice model.

### 2.2.1 Longitudinal PET-Imaging

Western blot analysis **(Figure S7)** confirmed that the human glioma astrocyte cells (U251) overexpressed the EGF receptor specific for the CTX.

Quantification of $^{89}$Zr-CTX in the brain was assessed by longitudinal PET-imaging at different time point (6min to 3 days post-injection) in U251 orthotopic model. At early time after injection (≤ 4h), based on PET images, a clearly higher amount of $^{89}$Zr-CTX was detected in the contralateral side of the group exposed to FUS than the control group (white arrow, **Figure 1A**). However, the maximal accumulation into the tumor occurred 24h after injection and stay constant up to 72h but did not differ between the groups (FUS vs no FUS). The amount of $^{89}$Zr-CTX into the tumor represented 5% of the injected dose (~ 50 µg of CTX/cm$^3$) and was 4-fold higher than in the contralateral side **(Figure 1B and C).**

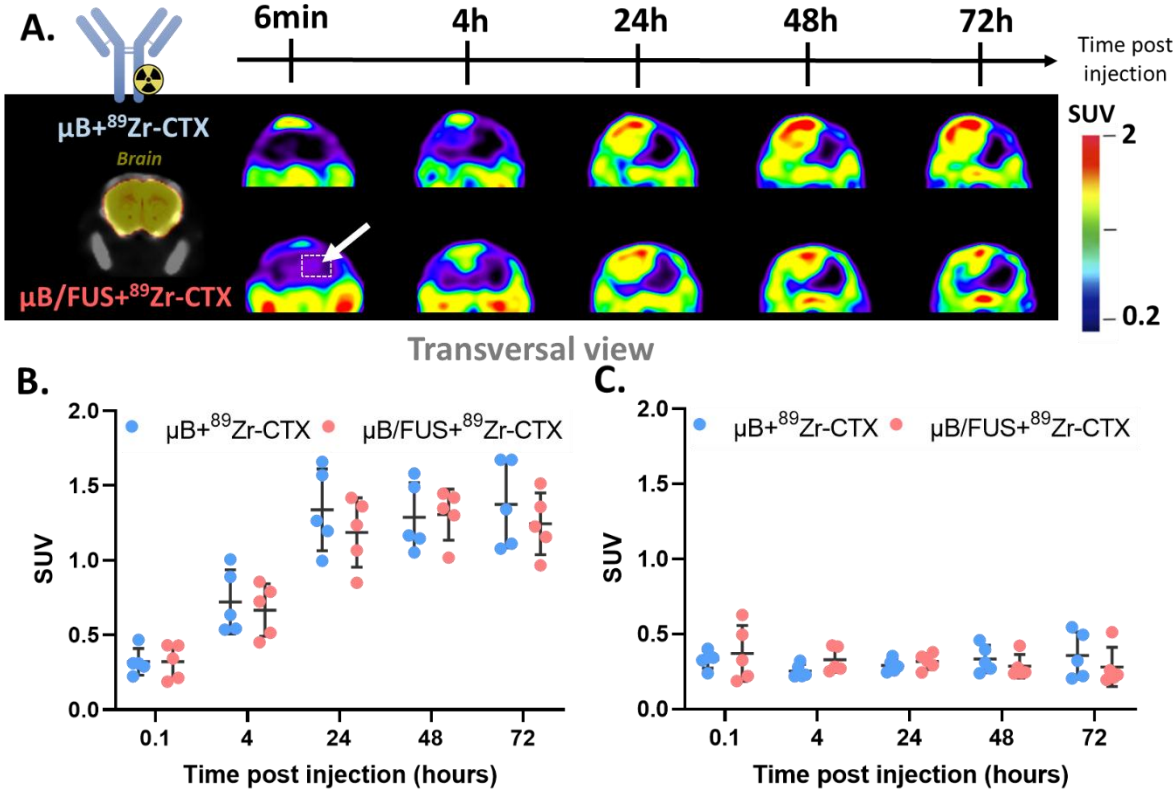

**Figure 1. Brain kinetics of $^{89}$Zr-CTX without (green) or with FUS (red) exposure. (A)** Transversal PET images obtained from mice brains without (top) or with FUS (bottom) at different time points (0.1h, 4h, 24h, 48h and 72h) after injection of $^{89}$Zr-CTX (40 mg/kg, 3.7 MBq). The white arrow shows the early broaden $^{89}$Zr-CTX brain delivery due to the FUS treatment. Quantitative $^{89}$Zr-CTX accumulated into the tumor **(B)** or the contralateral **(C)** other time. Data were extracted from a volume of interest of 13.3 mm$^3$ positioned in the middle of the tumor or the contralateral side. Results are represented as SUVmean ± standard deviation. No statistical difference was observed between the groups at any time after injection.

### 2.2.2 *Ex vivo* characterization of the impact of FUS on CTX delivery

The localization of $^{89}$Zr-CTX at the time to peak drug concentration (tmax = 24h for both groups post-injection) into the brain was assessed post-mortem via autoradiography and histological analysis. The visualization of the primary tumor was determined by hematoxylin-eosin staining **(Figure 2A).** The tumor localization was corroborated by the specific staining of human mitochondria and human EGFRp via immunofluorescence **(Figure 2B & Figure S8** respectively**).** Since U251 is issued from glioma astrocyte patient, an overexpression of the TSPO biomarker is expected.[37][38] The immunofluorescence straining of brain slices with anti-TSPO antibody, revealed not only the presence of a primary tumor area, but also a region with infiltrated tumor cells **(Figure 2B and S8).** The $^{89}$Zr-CTX accumulation into the brain slices was visualized by autoradiography **(Figure 2C).**

For the control group without FUS, the colocalization between autoradiography signal and the different histological staining (hematoxylin-eosin, human mitochondria, EGFRp and TSPO) confirmed the specific accumulation of $^{89}$Zr-CTX in the primary and unexpectedly into infiltrated tumor tissues. For the FUS group, $^{89}$Zr-CTX was able to reach every cell that expresses EGFR, even in the low infiltrative tumor area **(Figure 2D)**.

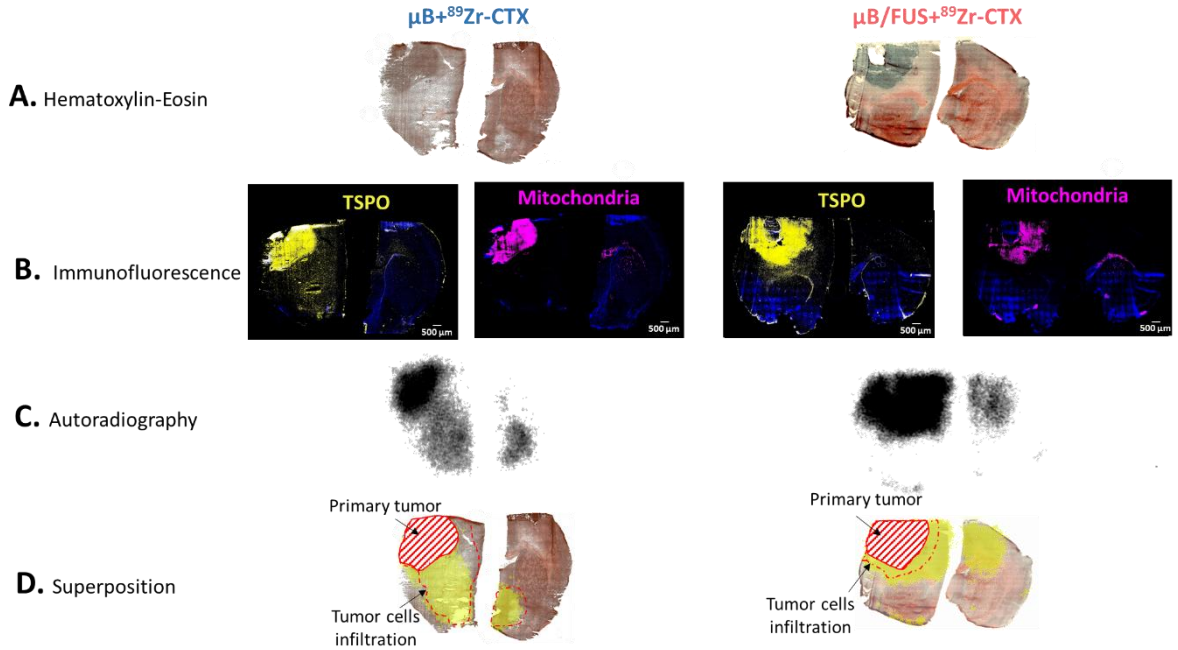


**Figure 2. Histological analyses obtained on adjacent slices from mice brains without (left) or with FUS (right) exposure, 24h after injection of $^{89}$Zr-CTX (40 mg/kg, 3.7 MBq). (A)** Hematoxylin-Eosin staining shows primary tumor area. **(B)** Immunofluorescence staining with anti-human mitochondria antibody (Alexa 488; *clone 113-1, MAB1273A4)* or anti-TSPO antibody (Alexa 546, EPR5384) shows primary and infiltrated tumor area. **(C)** Autoradiography shows $^{89}$Zr-CTX delivery into the brain. **(D)** Colocalization of primary (red strip) area or infiltrated (dashed line) tumor area and $^{89}$Zr-CTX delivery (yellow) area.

## 2.3 Does the neuroinflammation induced by FUS impact the brain delivery of CTX?

### 2.3.1 FUS-induced neuroinflammation: a longitudinal TSPO-PET imaging in healthy mice

Glial activation can be characterized by an increased expression of specific proteins such as the TSPO.[39][40] Previous study on healthy rat suggests that FUS increased glial cell activation into brain.[40] Since more than 70% of the cerebral immunity is preserved in the immunocompromised model, we wanted to evaluate the activation of glial cells induced by FUS exposure first in healthy mice and then in presence of the tumor overtime.[41] The immunologic deficiency of the nude mice model may present a limitation in terms of glial cell reduction but represents also a unique opportunity to assess tumor and FUS impact on the cerebral immunity. The temporal response of glial activation was assessed by quantifying TSPO expression using $^{18}$F-DPA-714 radioligand. The $^{18}$F-DPA-714 binding was observed to be significant at 48h post FUS and then decreasing at later time point **(Figure S9A).** This maximum $^{18}$F-DPA-714 was considered as the maximal impact of FUS on promoting glial activation. No difference in the time activity curve is observed before and after FUS, suggesting that the brain passage of $^{18}$F-DPA-714 does not depend on the integrity of the BBB **(Figure SI9B).**

### 2.3.2 In vivo evaluation of the impact of tumor cells, FUS and CTX treatment on neuroinflammation

The glial cells activation was then evaluated on the GBM bearing mice by carried out PET imaging at 48h post FUS treatment: (i) µB alone (n=4), (ii) µB with FUS (n=4), (iii) µB with CTX (n=4), (iv) CTX and µB with FUS (n=6).

Whatever the treatment condition, a 2-fold increase in the amount of $^{18}$F-DPA-714 was observed into the tumor region compared to the contralateral side taken as a reference region **(Figure 3).** On the tumor and contralateral side, FUS do not induce a significant increase of $^{18}$F-DPA-714 uptake **(Figure 3A&B).** However, five weeks of CTX treatment contributed to decrease the uptake of $^{18}$F-DPA-714 particularly significant in the contralateral compared to the control group with FUS exposure (1.5-fold, p=0.0384) or without FUS exposure (1.4-fold, p=0.0316).

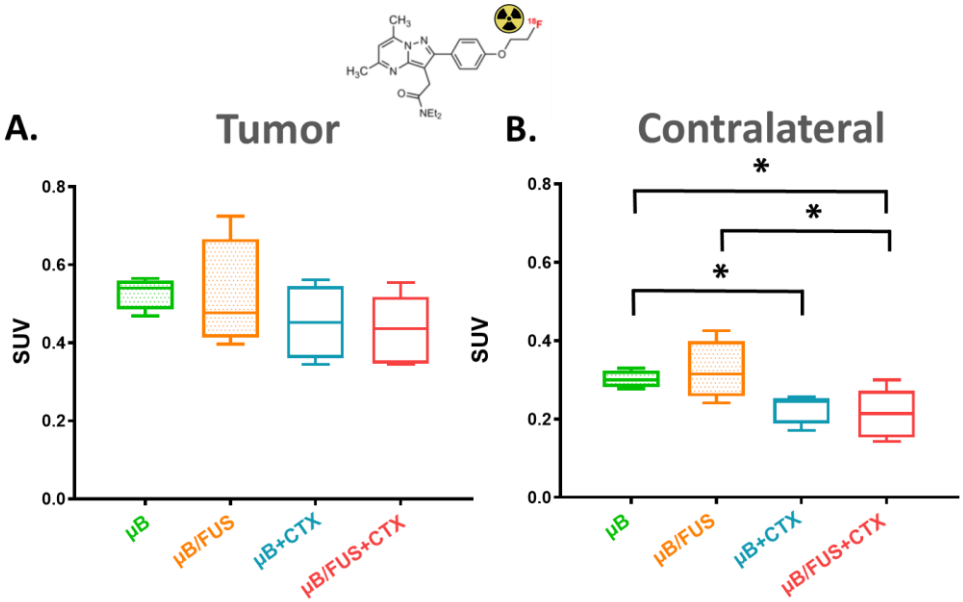


**Figure 3.** Quantitative $^{18}$F-DPA accumulated into the tumor **(A)** or the contralateral **(B)** 48h after the four treatment groups: (i) µB (n = 4), (ii) µB with FUS (n = 4), (iii) µB with CTX (n = 4), (iv) CTX and µB with FUS (n=6). Data were extracted from volumes of interests (VOIs) that were drawn manually around the tumor and then horizontally displaced in the contralateral side. Results are represented as SUVmean ± min and max. unpaired t-test were used for statistical significance of intergroup comparisons (*p<0.05)

### 2.3.3 *Ex vivo* Validation by TSPO colocalization between tumor versus glial cells obtained by immunofluorescence staining

The identification of the types of glial cells activated by immunofluorescence could be accessed by using specific proteins such as CD11B for microglia and glial fibrillary acidic protein (GFAP) for astrocytes. The qualitative expression levels of CD11B, GFAP and TSPO after 5 weeks of CTX combined with FUS exposure were evaluated by immunofluorescence on adjacent brain section.

The primary tumor localization was determined as previously described with anti-human mitochondria staining **(Figure 4Ab).** TSPO staining was mainly localized in the tumor area but also around the tumor ring **(Figure 4Aa and 4Ac).** CD11B staining revealed that microglia expression was restrained to the tumor ring **(Figure 4Ad).** GFAP staining revealed higher astrocytes expression in all tumor hemisphere compared to the contralateral hemisphere **(Figure 4Ae).** Images with higher objective were taken to access on glial cells morphology and protein co-localization, as illustrated in **Figure 4B.** The CD11B signal characteristic of microglia was colocalized with TSPO for most cells (white arrow). Astrocytes showed fibrous morphology characteristic of inflammatory stage with good colocalization between GFAP and TSPO inside the tumor (orange arrow) but not outside the tumor. However, the majority of TSPO expression inside the tumor was colocalized with neither GFAP nor CD11B signal.

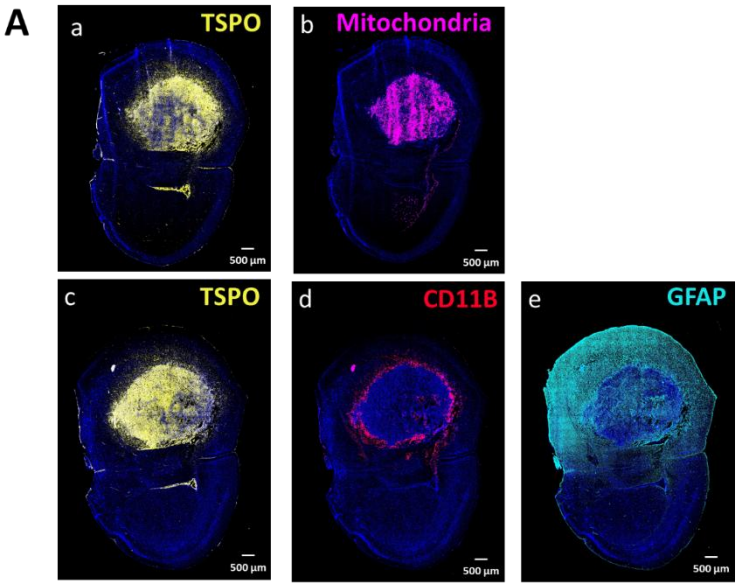

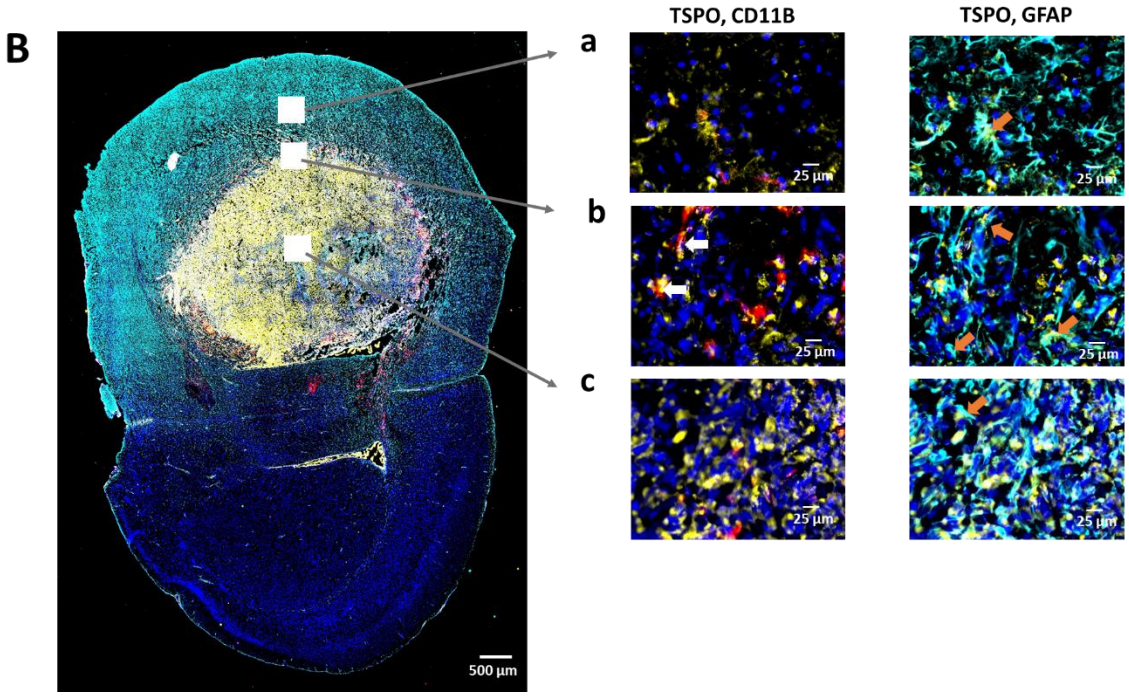


**Figure 4. Representative images from GBM bearing mice striatum 48h after the last CTX treatments combined with FUS exposure.** Bi-photonic scan of whole-brain sections stained for TSPO positive cells (microglia and astrocytes, yellow), CD11B positive cells (microglia, red), GFAP positive cells (astrocyte, cyan) and DAPI (blue) at low **(A)** and high magnification **(B)** in different brain areas: outside of the tumor (Ba), in the border of the tumor (Bb) and inside the tumor (Bc). White arrow shows CD11B colocalized with TSPO. Orange arrow shows GFAP colocalized with TSPO.

## 2.4 Repeated CTX combined with FUS-induce BBB opening did not improve overall survival in GBM mice

The efficiency of the different treatments was investigated on applying end-point score on animal survivance. The survival rate was interpreting using Kaplan-Meier survival curves **(Figure 6).** The statistical analysis after Mantel-Cox log-rank test is shown in **Table 1.**

Animals that received only FUS exposure did not show effective extension of survival (p=0.8936).

CTX improved the median survival time by 45% compared to the untreated group (42 days vs 29 days) but did not show any significant difference in terms of survival curve (p=0.1131). The survival curve of the CTX combined FUS exposure group was significantly different from the untreated group (p=0.0097) but did not differ from the CTX treatment alone (p>0.5%). Indeed, the median survival time was the same between the two groups (42 days). However, the mean survival was 30% longer than the untreated control group and 14% longer than the CTX alone group.

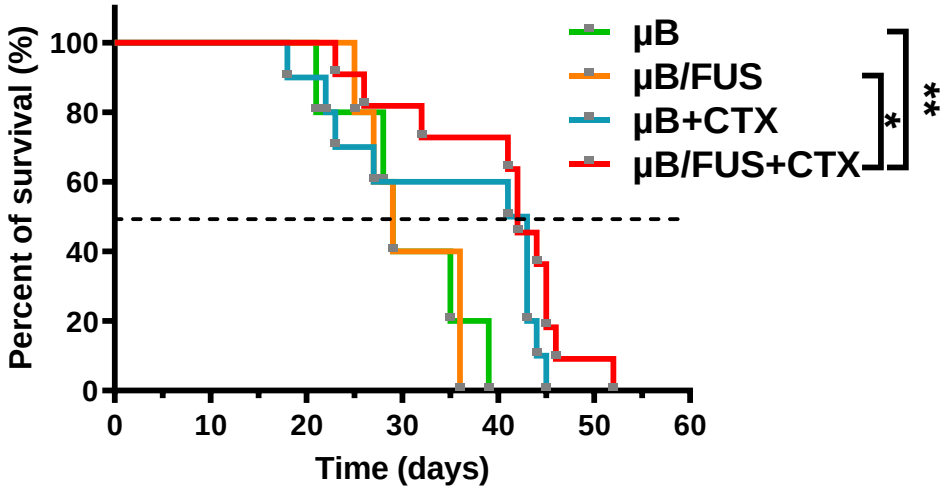


**Figure 6. Kaplan-Meier plot of survival for the different treatment groups**, (i) μB (n=7), (ii) μB with FUS (n=9), (iii) μB with CTX (n=10), (iv) CTX and μB with FUS (n=11). Mantel-Cox log-rank test was used for statistical significance of intergroup comparisons (*p<0.05, **p<0.01).

| Group | Median survival (d) | Increase in median survival time (%) | Mean survival (d) | Increase in mean survival time (%) | P value |
|---|---|---|---|---|---|
| μB | 29 | / | 30.40 ± 6.91 | / | / |
| μB/FUS | 29 | 0 | 30.60 ± 5.13 | 0.66 | 0.8936 |
| μB+CTX | 42 | 44.83 | 34.90 ± 10.93 | 14.80 | 0.1131 |
| μB/FUS+CTX | 42 | 44.83 | 39.82 ± 8.97 | 30.99 | 0.0097 |

**Table 1. Summary of Animal survival Analysis.** Results are represented as mean ± standard deviation.

# DISCUSSION

The different treatment failure to improve the glioblastoma patient care led to evaluate untapped potential novel cancer therapy strategies. Within this context, we investigated the benefit of repeated CTX monotherapy on nude mice orthotopically grafted with human glioma cells (U251) that overexpress EGFR. The main question on CTX to treat efficiently GBM-EGFR$^{+}$ is the degree to which intravenous delivery of this large monoclonal antibody (~ 150 kDa) crosses the BBB/BTB. ImmunoPET imaging with $^{89}$Zr-CTX has been demonstrated to be an efficient predictive biomarker of anti-EGFR treatment efficacy.[42] In U251 orthotopic model, $^{89}$Zr-CTX tumoral uptake was impressive (at 24 h post-injection, SUV=1.19±0.23), leading to a 4 time higher tumoral uptake compared to the healthy brain tissue. In terms of pharmacodynamic, the concentration of CTX remained stable into the tumor up to 3 days post-injection. This long-term CTX accumulation within the tumor explained the efficacy of repeated CTX treatments, every three to four days, with an 45% increased of the mice bearing tumor median survival time. However, the overall survival time was not significantly different, suggesting a mild tumor response at the mAb treatment. Former preclinical study by Greenall *et al*. using three CTX treatments (one treatment per week) on mice orthotopically grafted with patient-derived glioblastoma cell have demonstrated a small (5 days, $p<0.05$) improvement in survival compared to control group.[12] For optimal CTX efficacy, preclinical[15][43] and clinical[44][45] studies highlight the importance of delivering CTX at a level which nearly completely saturates EGFR within the tumor. T.Martens *et al.* observed a significant tumor growth inhibition when 55 µg of the CTX were daily administrated using osmotic minipumps directly into EGFR positive orthotopic xenografts mice.[15] In the present study, the dose of CTX delivered, which correspond at 50 µg.cm$^{-3}$ every 3 days, might be insufficient to observe a clear therapeutic effect of the CTX treatment alone.

To increase significantly the accumulation of the CTX, FUS is one of technic that has been promising to increase by two the amount of CTX in healthy brain.[28] The PET images of $^{89}$Zr-CTX with and without FUS treatment confirmed that FUS clearly increased early extravasation until 4h post injection. FUS allowed broaden delivery of $^{89}$Zr-CTX around the tumor to assess all the EGFR tumor cell, as demonstrated by autoradiography combined with histological analysis obtained 24h post injection**.** As a result, CTX might have been delivered more homogeneously into the primary tumor and may also reach eventually infiltrated tumor cells present in the contralateral hemisphere, at early time points.

However, BBB/BTB opening with FUS did not significantly enhance the amount of CTX that could reach the tumor itself compared to the group without FUS, at any selected time-point. The limited added value of FUS on survival impact is consistent with this observation**.** The use of CTX combined with FUS does not additionally improve nor the overall and neither the mean survival time of the mice compared to the CTX treatment alone. As FUS-induced BBB/BTB opening is a transient phenomenon, we could first hypothesize that the early additional amount of mAb delivered into the brain may still be too low to induce a therapeutic effect. But the fact that the amount of CTX delivered into the tumor slightly increase to reach very fast a plateau at the same level with or without FUS may indicate that the maximum CTX delivery was achieved. The BTB status might more likely, already be substantially impaired by the presence of the tumor in this condition. *Ex vivo* analysis carried out on the brain of a mouse not exposed to FUS revealed the presence of $^{89}$Zr-CTX into primary and infiltrated tumor cells, thus confirming natural BTB/BBB leakiness to CTX, even in the absence of FUS**.** Indeed, glioma migration along the blood vessels can induce local destabilization of the vessels remodeling the BBB/BTB.[11][44] This allows the passage of mAb in the infiltrative part of the GBM. The vessel destabilization certainly engages a complete tumor penetration of the antibody is enough to saturate the target, as suggested by Freeman et al.[47] This explains the temporary early increase of TRZ delivery not observed at the latest time point[48] or the absence of TRZ therapeutically benefit [23][24] in prior studies using TRZ combined with FUS on rodents brain metastases models.

A different hypothesize of the lack of CTX efficacy can lean on the inflammation impact. The development and the progression of the tumor has been widely shown to influence also the

neuroinflammation.[49] Several groups have studied the role of FUS on temporary activation of glial cells.[25][26] It is well known that glial cells activated generate a cascade of mechanisms associated with inflammatory effects, such as phagocytose.[50][51] Activation of glial cells by FUS exposure could induce a cytotoxic environment for GBM and then influence the therapeutic efficacy of CTX. Therefore, we were also interested in evaluating the capacity of FUS to activate the microglia and the astrocyte.

The increased expression of TSPO measured by PET imaging using specific radiopharmaceutical tracer, such as $^{18}$F-DPA-714, has demonstrated to be a potent biomarker for inflammatory microglia[52][53][54] and astrocytes[55][54]. Using TSPO-PET imaging, we first confirmed in healthy mice brains that FUS-mediated BBB opening is accompanied by the temporary activation of glial cells, as expected.[25][26] Glial cells activity significantly increased during two days and then slowly decreased and returned to their initial levels four days after FUS exposure.

In our GBM mice model, the effect of the FUS on glial cells activation was more subtle. On the contralateral hemisphere a broaden TSPO signal was observed for the FUS exposure groups compared to the unexposed groups without significance**.** Interestingly, repeated CTX treatments with or without FUS exposure induce a significative decrease of the TSPO signal in the contralateral hemisphere. Therefore, CTX itself may also influence the glial cells state. However, on the tumor hemisphere no significant difference in TSPO expression was observed between the four treatment groups. We hypothesis that the high TSPO signal from the tumor cell itself can flatten the activation of glial cells followed by FUS exposure. To verify this assumption, immunofluorescence staining of active glial cells, specifically CD11B for microglia and GFAP for astrocytes, and their colocalization with TSPO expression were evaluated on brain slide of a mouse treated with both CTX and FUS. A good colocalization between GFAP with TSPO inside the tumor and CD11B with TSPO just around the tumor indicated the infiltration of inflammatory astrocytes into the tumor whereas inflammatory microglia were restricted to the tumor boarder. Despite this finding, the expression of TSPO by the glial cells was well below the number of tumor cells that have been shown to express also TSPO. Our results are consistent with studies revealing that TSPO is predominantly expressed in neoplastic cells with only a subpopulation of glial cells contributing to PET signal.[36] In addition, a surprisingly high level of astrocytes with fibrous morphology and GFAP expression characteristics of inflammatory stage were present outside the tumor in all the hemisphere. However, they did not overexpress TSPO. For all these reasons, the low difference of $^{18}$F-DPA-714 uptake between treatment groups can be linked to a small subset of glial activation in this GBM model. Deeper histological investigations with additional markers and under numerous animals will be necessary to obtain semi-quantitative results on glial inflammatory state and to evaluate accurately the impact of the FUS on glial cells. However, we can estimate at this stage that glial cell activation under FUS could have a negligeable impact on the CTX efficacy.

# CONCLUSION

We confirmed that FUS in combination with µB induces a larger BBB and BTB opening around the tumor at early time points. However, we demonstrated that if the BTB is sufficiently permeable to CTX, FUS cannot further improve the accumulation and retention of CTX into the tumor. In addition, activation of the glial cells following FUS was too low and too transient to induce a cytotoxic environment for GBM. This may explain the low impact of CTX combined with FUS in this situation. As a conclusion, in our model of GBM, FUS did no exacerbate an impact of immunotherapy. From a clinical perspective, this study suggests a key role for non-invasive techniques such as immuno-PET to stratify patients according to their BTB impairment before considering the use of mAb treatment alone or combined with FUS.

# ACKNOWLEDGEMENTS

The authors acknowledge the financial support from ITMO Cancer of Aviesan on funds administered by Inserm ($IM^2FUS$ Grant). The authors would like to thank Yoan Fontyn and Vincent Brulon for technical support during the acquisitions and reconstructions of PET(CT) images, Fabien Rastello and Georges Willoquet for informatics support and Laurène Jourdain for the 3D printing devices (Laboratoire d'Imagerie Biomédicale Multimodale Paris Saclay). This work was performed on a platform member of France Life Imaging network (grant ANR692 11-INBS-0006).

# REFERENCES

[1] N. Grech, T. Dalli, S. Mizzi, L. Meilak, N. Calleja, et A. Zrinzo, « Rising Incidence of Glioblastoma Multiforme in a Well-Defined Population », *Cureus*, mai 2020, doi: 10.7759/cureus.8195.

[2] H. K. Gan, A. N. Cvrljevic, et T. G. Johns, « The epidermal growth factor receptor variant III (EGFRvIII): where wild things are altered », *FEBS J.*, vol. 280, n° 21, p. 5350‑5370, nov. 2013, doi: 10.1111/febs.12393.

[3] P. M. Harari, « Epidermal growth factor receptor inhibition strategies in oncology », *Endocr. Relat. Cancer*, vol. 11, n° 4, p. 689‑708, déc. 2004, doi: 10.1677/erc.1.00600.

[4] R. S. Herbst et D. M. Shin, « Monoclonal antibodies to target epidermal growth factor receptor-positive tumors: A new paradigm for cancer therapy », *Cancer*, vol. 94, n° 5, p. 1593‑1611, mars 2002, doi: 10.1002/cncr.10372.

[5] D. Patel *et al.*, « Monoclonal antibody cetuximab binds to and down-regulates constitutively activated epidermal growth factor receptor vIII on the cell surface », *Anticancer Res.*, vol. 27, n° 5A, p. 3355‑3366, oct. 2007.

[6] S. K. A. Blick et L. J. Scott, « Cetuximab: A Review of its Use in Squamous Cell Carcinoma of the Head and Neck and Metastatic Colorectal Cancer », *Drugs*, vol. 67, n° 17, p. 2585‑2607, 2007, doi: 10.2165/00003495-200767170-00008.

[7] M. H. Yazdi, M. A. Faramarzi, S. Nikfar, et M. Abdollahi, « A Comprehensive Review of Clinical Trials on EGFR Inhibitors Such as Cetuximab and Panitumumab as Monotherapy and in Combination for Treatment of Metastatic Colorectal Cancer », *Avicenna J. Med. Biotechnol.*, vol. 7, n° 4, p. 134‑144, déc. 2015.

[8] D. J. Jonker *et al.*, « Cetuximab for the Treatment of Colorectal Cancer », *N. Engl. J. Med.*, vol. 357, n° 20, p. 2040‑2048, nov. 2007, doi: 10.1056/NEJMoa071834.

[9] J. L. Eller, S. L. Longo, D. J. Hicklin, et G. W. Canute, « Activity of Anti-epidermal Growth Factor Receptor Monoclonal Antibody C225 against Glioblastoma Multiforme », *Neurosurgery*, vol. 51, n° 4, p. 1005‑1014, oct. 2002, doi: 10.1097/00006123-200210000-00028.

[10] M. Westphal, C. L. Maire, et K. Lamszus, « EGFR as a Target for Glioblastoma Treatment: An Unfulfilled Promise », *CNS Drugs*, vol. 31, n° 9, p. 723‑735, sept. 2017, doi: 10.1007/s40263-017-0456-6.

[11] C. D. Arvanitis, G. B. Ferraro, et R. K. Jain, « John F. Deeken, Clinical Cancer research, 2007 », *Nat. Rev. Cancer*, vol. 20, n° 1, p. 26‑41, janv. 2020, doi: 10.1038/s41568-019-0205-x.

[12] S. A. Greenall *et al.*, « Most clinical anti-EGFR antibodies do not neutralize both wtEGFR and EGFRvIII activation in glioma », *Neuro-Oncol.*, vol. 21, n° 8, p. 1016‑1027, août 2019, doi: 10.1093/neuonc/noz073.

[13] J. R. Kane, « The Role of Brain Vasculature in Glioblastoma », *Mol. Neurobiol.*, vol. 56, n° 9, p. 6645‑6653, sept. 2019, doi: 10.1007/s12035-019-1561-y.

[14] J. N. Sarkaria *et al.*, « Is the blood–brain barrier really disrupted in all glioblastomas? A critical assessment of existing clinical data », *Neuro-Oncol.*, vol. 20, n° 2, p. 184‑191, janv. 2018, doi: 10.1093/neuonc/nox175.

[15] T. Martens *et al.*, « Inhibition of Glioblastoma Growth in a Highly Invasive Nude Mouse Model Can Be Achieved by Targeting Epidermal Growth Factor Receptor but not Vascular Endothelial

Growth Factor Receptor-2 », *Clin. Cancer Res.*, vol. 14, n° 17, p. 5447‑5458, sept. 2008, doi: 10.1158/1078-0432.CCR-08-0147.
[16] S. Chakraborty *et al.*, « Superselective intraarterial cerebral infusion of cetuximab after osmotic blood/brain barrier disruption for recurrent malignant glioma: phase I study », *J. Neurooncol.*, vol. 128, n° 3, p. 405‑415, juill. 2016, doi: 10.1007/s11060-016-2099-8.
[17] « Super-selective Intra-arterial Repeated Infusion of Cetuximab for the Treatment of Newly Diagnosed Glioblastoma - Full Text View - ClinicalTrials.gov ».
[18] A. Burgess, K. Shah, O. Hough, et K. Hynynen, « Focused ultrasound-mediated drug delivery through the blood–brain barrier », *Expert Rev. Neurother.*, vol. 15, n° 5, p. 477‑491, mai 2015, doi: 10.1586/14737175.2015.1028369.
[19] A. Dauba *et al.*, « Recent Advances on Ultrasound Contrast Agents for Blood-Brain Barrier Opening with Focused Ultrasound », *Pharmaceutics*, vol. 12, n° 11, p. 1125, nov. 2020, doi: 10.3390/pharmaceutics12111125.
[20] M. Kinoshita, N. McDannold, F. A. Jolesz, et K. Hynynen, « Noninvasive localized delivery of Herceptin to the mouse brain by MRI-guided focused ultrasound-induced blood-brain barrier disruption », *Proc. Natl. Acad. Sci.*, vol. 103, n° 31, p. 11719‑11723, août 2006, doi: 10.1073/pnas.0604318103.
[21] V. L. Tran *et al.*, « Impact of blood-brain barrier permeabilization induced by ultrasound associated to microbubbles on the brain delivery and kinetics of cetuximab: An immunoPET study using 89Zr-cetuximab », *J. Controlled Release*, vol. 328, p. 304‑312, déc. 2020, doi: 10.1016/j.jconrel.2020.08.047.
[22] H.-L. Liu *et al.*, « Focused Ultrasound Enhances Central Nervous System Delivery of Bevacizumab for Malignant Glioma Treatment », *Radiology*, vol. 281, n° 1, p. 99‑108, oct. 2016, doi: 10.1148/radiol.2016152444.
[23] E.-J. Park, Y.-Z. Zhang, N. Vykhodtseva, et N. McDannold, « Ultrasound-mediated blood-brain/blood-tumor barrier disruption improves outcomes with trastuzumab in a breast cancer brain metastasis model », *J. Controlled Release*, vol. 163, n° 3, p. 277‑284, nov. 2012, doi: 10.1016/j.jconrel.2012.09.007.
[24] T. Kobus, I. K. Zervantonakis, Y. Zhang, et N. J. McDannold, « Growth inhibition in a brain metastasis model by antibody delivery using focused ultrasound-mediated blood-brain barrier disruption », *J. Controlled Release*, vol. 238, p. 281‑288, sept. 2016, doi: 10.1016/j.jconrel.2016.08.001.
[25] Z. I. Kovacs *et al.*, « Disrupting the blood–brain barrier by focused ultrasound induces sterile inflammation », *Proc. Natl. Acad. Sci.*, vol. 114, n° 1, p. E75‑E84, janv. 2017, doi: 10.1073/pnas.1614777114.
[26] J. F. Jordão *et al.*, « Amyloid-β plaque reduction, endogenous antibody delivery and glial activation by brain-targeted, transcranial focused ultrasound », *Exp. Neurol.*, vol. 248, p. 16‑29, oct. 2013, doi: 10.1016/j.expneurol.2013.05.008.
[27] Y. W. S. Jauw *et al.*, « Immuno-Positron Emission Tomography with Zirconium-89-Labeled Monoclonal Antibodies in Oncology: What Can We Learn from Initial Clinical Trials? », *Front. Pharmacol.*, vol. 7, mai 2016, doi: 10.3389/fphar.2016.00131.
[28] V. L. Tran *et al.*, « Impact of blood-brain barrier permeabilization induced by ultrasound associated to microbubbles on the brain delivery and kinetics of cetuximab: An immunoPET study using 89Zr-cetuximab », *J. Controlled Release*, vol. 328, p. 304‑312, déc. 2020, doi: 10.1016/j.jconrel.2020.08.047.
[29] M. J. W. D. Vosjan *et al.*, « Conjugation and radiolabeling of monoclonal antibodies with zirconium-89 for PET imaging using the bifunctional chelate p-isothiocyanatobenzyl-desferrioxamine », *Nat. Protoc.*, vol. 5, n° 4, p. 739‑743, avr. 2010, doi: 10.1038/nprot.2010.13.
[30] J. Fukai, K. Nishio, T. Itakura, et F. Koizumi, « Antitumor activity of cetuximab against malignant glioma cells overexpressing EGFR deletion mutant variant III », *Cancer Sci.*, sept. 2008, doi: 10.1111/j.1349-7006.2008.00945.x.

[31] S. L. Gibbs-Strauss *et al.*, « Detecting Epidermal Growth Factor Receptor Tumor Activity In Vivo During Cetuximab Therapy of Murine Gliomas », *Acad. Radiol.*, vol. 17, n° 1, p. 7‑17, janv. 2010, doi: 10.1016/j.acra.2009.07.027.
[32] M.-S. Felix *et al.*, « Ultrasound-Mediated Blood-Brain Barrier Opening Improves Whole Brain Gene Delivery in Mice », *Pharmaceutics*, vol. 13, n° 8, p. 1245, août 2021, doi: 10.3390/pharmaceutics13081245.
[33] G. Hugon *et al.*, « [18F]2-Fluoro-2-deoxy-sorbitol PET Imaging for Quantitative Monitoring of Enhanced Blood-Brain Barrier Permeability Induced by Focused Ultrasound », *Pharmaceutics*, vol. 13, n° 11, p. 1752, oct. 2021, doi: 10.3390/pharmaceutics13111752.
[34] A. Damont *et al.*, « Radiosynthesis of [ $^{18}$ F]DPA-714, a selective radioligand for imaging the translocator protein (18 kDa) with PET », *J. Label. Compd. Radiopharm.*, vol. 51, n° 7, p. 286‑292, juin 2008, doi: 10.1002/jlcr.1523.
[35] A. E. Dorr, J. P. Lerch, S. Spring, N. Kabani, et R. M. Henkelman, « High resolution three-dimensional brain atlas using an average magnetic resonance image of 40 adult C57Bl/6J mice », *NeuroImage*, vol. 42, n° 1, p. 60‑69, août 2008, doi: 10.1016/j.neuroimage.2008.03.037.
[36] Z. Su *et al.*, « The 18-kDa Mitochondrial Translocator Protein in Human Gliomas: An $^{11}$ C-( *R* )PK11195 PET Imaging and Neuropathology Study », *J. Nucl. Med.*, vol. 56, n° 4, p. 512‑517, avr. 2015, doi: 10.2967/jnumed.114.151621.
[37] H. Pigeon *et al.*, « TSPO-PET and diffusion-weighted MRI for imaging a mouse model of infiltrative human glioma », *Neuro-Oncol.*, vol. 21, n° 6, p. 755‑764, juin 2019, doi: 10.1093/neuonc/noz029.
[38] B. Zinnhardt *et al.*, « Combined PET Imaging of the Inflammatory Tumor Microenvironment Identifies Margins of Unique Radiotracer Uptake », *Cancer Res.*, vol. 77, n° 8, p. 1831‑1841, avr. 2017, doi: 10.1158/0008-5472.CAN-16-2628.
[39] E. L. Werry *et al.*, « Recent Developments in TSPO PET Imaging as A Biomarker of Neuroinflammation in Neurodegenerative Disorders », *Int. J. Mol. Sci.*, vol. 20, n° 13, p. 3161, juin 2019, doi: 10.3390/ijms20133161.
[40] S. Sinharay *et al.*, « In vivo imaging of sterile microglial activation in rat brain after disrupting the blood-brain barrier with pulsed focused ultrasound: [18F]DPA-714 PET study », *J. Neuroinflammation*, vol. 16, n° 1, p. 155, déc. 2019, doi: 10.1186/s12974-019-1543-z.
[41] W.-W. Htain, S.-K. Leong, et E.-A. Ling, « A qualitative and quantitative study of the glial cells in normal and athymic mice », *Glia*, vol. 15, n° 1, p. 11‑21, 1995, doi: 10.1002/glia.440150103.
[42] A. J. G. Even *et al.*, « Quantitative assessment of Zirconium-89 labeled cetuximab using PET/CT imaging in patients with advanced head and neck cancer: a theragnostic approach », *Oncotarget*, vol. 8, n° 3, p. 3870‑3880, déc. 2016, doi: 10.18632/oncotarget.13910.
[43] S. A. Greenall *et al.*, « Most clinical anti-EGFR antibodies do not neutralize both wtEGFR and EGFRvIII activation in glioma », *Neuro-Oncol.*, vol. 21, n° 8, p. 1016‑1027, août 2019, doi: 10.1093/neuonc/noz073.
[44] J. Baselga *et al.*, « Phase I Studies of Anti–Epidermal Growth Factor Receptor Chimeric Antibody C225 Alone and in Combination With Cisplatin », *J. Clin. Oncol.*, vol. 18, n° 4, p. 904‑904, févr. 2000, doi: 10.1200/JCO.2000.18.4.904.
[45] B. Neyns *et al.*, « Stratified phase II trial of cetuximab in patients with recurrent high-grade glioma », *Ann. Oncol.*, vol. 20, n° 9, p. 1596‑1603, sept. 2009, doi: 10.1093/annonc/mdp032.
[46] Y. Wang *et al.*, « Remodelling and Treatment of the Blood-Brain Barrier in Glioma », *Cancer Manag. Res.*, vol. Volume 13, p. 4217‑4232, mai 2021, doi: 10.2147/CMAR.S288720.
[47] D. J. Freeman *et al.*, « Tumor penetration and epidermal growth factor receptor saturation by panitumumab correlate with antitumor activity in a preclinical model of human cancer », *Mol. Cancer*, vol. 11, n° 1, p. 47, juill. 2012, doi: 10.1186/1476-4598-11-47.
[48] C. D. Arvanitis *et al.*, « Mechanisms of enhanced drug delivery in brain metastases with focused ultrasound-induced blood–tumor barrier disruption », *Proc. Natl. Acad. Sci.*, vol. 115, n° 37, p. E8717‑E8726, sept. 2018, doi: 10.1073/pnas.1807105115.

[49] A. Mantovani, P. Allavena, A. Sica, et F. Balkwill, « Cancer-related inflammation », *Nature*, vol. 454, n° 7203, p. 436‑444, juill. 2008, doi: 10.1038/nature07205.
[50] J. Dimitrova-Shumkovska, L. Krstanoski, et L. Veenman, « Diagnostic and Therapeutic Potential of TSPO Studies Regarding Neurodegenerative Diseases, Psychiatric Disorders, Alcohol Use Disorders, Traumatic Brain Injury, and Stroke: An Update », *Cells*, vol. 9, n° 4, p. 870, avr. 2020, doi: 10.3390/cells9040870.
[51] E. L. Werry *et al.*, « Recent Developments in TSPO PET Imaging as A Biomarker of Neuroinflammation in Neurodegenerative Disorders », *Int. J. Mol. Sci.*, vol. 20, n° 13, p. 3161, juin 2019, doi: 10.3390/ijms20133161.
[52] L. Beckers *et al.*, « Increased Expression of Translocator Protein (TSPO) Marks Pro-inflammatory Microglia but Does Not Predict Neurodegeneration », *Mol. Imaging Biol.*, vol. 20, n° 1, p. 94‑102, févr. 2018, doi: 10.1007/s11307-017-1099-1.
[53] L. Vivash et T. J. O'Brien, « Imaging Microglial Activation with TSPO PET: Lighting Up Neurologic Diseases? », *J. Nucl. Med.*, vol. 57, n° 2, p. 165‑168, févr. 2016, doi: 10.2967/jnumed.114.141713.
[54] M. Pannell *et al.*, « Imaging of translocator protein upregulation is selective for pro-inflammatory polarized astrocytes and microglia », *Glia*, vol. 68, n° 2, p. 280‑297, févr. 2020, doi: 10.1002/glia.23716.
[55] S. Lavisse *et al.*, « Reactive Astrocytes Overexpress TSPO and Are Detected by TSPO Positron Emission Tomography Imaging », *J. Neurosci.*, vol. 32, n° 32, p. 10809‑10818, août 2012, doi: 10.1523/JNEUROSCI.1487-12.2012.